

Efficient CUF-based method for the vibrations of thin-walled open cross-section beams under compression

Original

Efficient CUF-based method for the vibrations of thin-walled open cross-section beams under compression / Augello, R.; Daneshkhah, E.; Xu, X.; Carrera, E.. - In: JOURNAL OF SOUND AND VIBRATION. - ISSN 0022-460X. - 510:(2021), p. 116232. [10.1016/j.jsv.2021.116232]

Availability:

This version is available at: 11583/2922736 since: 2021-09-09T20:45:43Z

Publisher:

Academic Press

Published

DOI:10.1016/j.jsv.2021.116232

Terms of use:

This article is made available under terms and conditions as specified in the corresponding bibliographic description in the repository

Publisher copyright

(Article begins on next page)

Efficient CUF-based method for the vibrations of thin-walled open cross-section beams under compression

Riccardo Augello^{a,*}, Ehsan Daneshkhah^{a,†}, Xiangyang Xu^{b,‡}, Erasmo Carrera^{a,c,§},

^aMul² Group, Department of Mechanical and Aerospace Engineering,
Politecnico di Torino, 10129 Torino, Italy

^bSchool of rail transportation, Soochow University, Suzhou, China

^cDepartment of mechanical engineering, College of engineering,
Prince Mohammad Bin Fahd University P.O. Box 1664. Al Khobar 31952.
Kingdom of Saudi Arabia

Abstract: This study proposes an efficient method for the evaluation of vibrations and buckling in thin-walled beams with complex geometries subjected to progressive compressive loads. A comprehensive study is conducted in order to investigate the effects of compressive loads on the natural frequencies of the thin-walled beams. Namely, a numerical simulation of the Vibration Correlation Technique is provided in this study. Finite Elements (FEs) are built in the framework of the Carrera Unified Formulation (CUF), and the displacements of complex geometric shapes of the thin-walled beams are evaluated using low- to higher-order Taylor and Lagrange polynomials. The results are compared with the experimental results of the available literature and the numerical results by the shell models. The cross-sectional deformations of the beam due to the vibration modes are also compared, and the importance of structural theories capable of accurate detection of complex cross-sectional deformations is highlighted. The obtained results are demonstrated to be promising and accurate and match reasonably well with the experiments and shell models, which are more expensive in terms of computational costs compared to the efficient CUF ones proposed here.

Keywords: Vibration analysis; Carrera Unified Formulation; Thin-walled beam structures; Compressive loads; Vibration Correlation Technique.

1 Introduction

Thin-walled beam structures with open cross-sections are widely used in different applications such as mechanical, aerospace, and civil engineering. Beams are structures with one dimension much larger than the other two and primarily subjected to lateral loads, resulting in the bending of their reference axes [1]. One-dimensional beam theories were developed due to the simplicity and lower computational costs. Beam theories were initially formulated by Euler [2], Bernoulli [3], Timoshenko [4, 5], and further by Saint-Venant [6, 7]. Dynamic behaviors of thin-walled beams by using experimental, numerical, and analytical approaches were investigated [8, 9]. In many cases, the beam, columns, and plate structures are subjected to axial compression [10, 11, 12]. Therefore, the accurate

*Research assistant. E-mail: riccardo.augello@polito.it

†Ph.D. student. E-mail: ehsan.daneshkhah@polito.it

‡Full Professor. E-mail: x.y.xu@suda.edu.cn

§Full Professor. E-mail: erasmo.carrera@polito.it

understanding of the vibration and buckling of these structures under compression plays a pivotal role in the safe and reliable engineering design. The Vibration Correlation Technique (VCT) [13] was introduced as a non-destructive method to evaluate buckling loads of structures under progressive compressive loads. According to the VCT, the natural frequencies of the structure are decreased by the compressive loads. By the assumption that the vibration modes are similar to the buckling ones, the critical buckling load can be extrapolated as the load which causes zero natural frequency [14]. A review paper by Abramovich [15] studied the use of the VCT for buckling load prediction of thin-walled structures, including the available literature for different structures such as columns, beams, plates, panels, and cylindrical shells.

Vibration and buckling of beam structures under compression were investigated by many researchers [16, 17, 18, 19]. Abramovich [20] studied the natural frequencies in the Timoshenko beams with different boundary conditions subjected to compressive axial loads. Prokic [21] worked on the flexure-torsion coupled vibrations of axially loaded thin-walled beams by exact solutions. Carpinteri et al. [22] studied the evolution of fundamental frequency in slender beams under axial displacements, and analyzed the effects of geometrical imperfections and constraint conditions. Some research studies are focused on the double-beam systems under compressive axial loads [23, 24]. Piana et al. [25] worked on the buckling and natural frequencies of non-symmetric thin-walled beams. They used a universal machine for the experimental compression tests that imposed a relative axial displacement in the ends of the aluminum thin-walled beams. The same authors worked on the thin-walled beams with symmetric cross-sections considering the warping effects [26]. Aquaro [27] focused on the torsional instabilities of thin-walled open cross-section beams with stiffeners placed in different positions. Zmuda [28] presented a numerical analysis on the axially-loaded steel beams and considered linearly-elastic and elastic-perfectly plastic material behaviors for the cold-formed lipped channel section beams. Elkaimbillah et al. [29] proposed a one-dimensional finite element (FE) model for the forced nonlinear vibration response of thin-walled composite beams with open variable cross-sections. Cabral et al. [14] used the VCT for the experimental and numerical analysis of pre-stressed laminated reinforced panels. The results of experimental tests were compared by advanced FE models using the Carrera Unified Formulation (CUF). By using the CUF, Pagani et al. [30] worked on the VCT for analysis of beam structures in the geometrical nonlinear framework.

The CUF was demonstrated as an efficient and accurate method to solve the vibration analysis problems of structures [31, 32, 33]. A hierarchical FE by using the CUF was presented by Carrera et al. [34]. Mass and stiffness matrices of the structure in terms of the independent fundamental nuclei were formulated. Petrolo et al. [35] investigated the free vibration response of compact and bridge-like cross-sections. The higher-order theories based on the CUF were used for the free vibration response of different beam cross-sections [36]. By opportunely modifying the fundamental nucleus of the mass matrix, Pagani et al. [37] evaluated the effect of nonstructural localized inertia on the free vibration response of thin-walled structures. Dan et al. [38] studied the free vibration of simply supported beams with solid and thin-walled cross-sections using the CUF. Xu et al. [39] used Lagrange polynomial expansion for the free vibration analysis of thin-walled beams, and presented an efficient FE method based on the CUF. Pagani et al. [40] investigated the frequency and mode change of beam structures subjected to geometrical nonlinearities in the large displacements and rotations. They focused on the large-deflection and post-buckling of different compact and thin-walled beams. Furthermore, the influence of large-displacements on the vibration of composite beams was evaluated [41].

In this paper, an efficient CUF-based method for evaluating vibrations and buckling in the thin-walled beams with complex open cross-sections subjected to progressive compressive loads is presented. A comprehensive study is conducted in order to investigate the effect of compressive loads on the natural frequencies of the beams subjected to progressive compressive loads. The CUF-based FEs with the Taylor and Lagrange expansions are implemented and compared with the experimental results of the available literature and the numerical results by the shell models. Moreover, the cross-sectional deformations of the beam due to the vibration modes are compared, and the importance

of structural theories capable of accurate detection of these cross-sectional deformations is outlined. The obtained results by the CUF-based FE method correlate reasonably well with the experiments and shell models, which are considerably more expensive in terms of computational costs.

2 Basic considerations

By considering a generic beam with the cross-section domain A in the $x - z$ plane, and the axis along the y direction, the displacement, stress, and the strain vectors can be defined in the following vectorial forms:

$$\begin{aligned}\mathbf{u}(x, y, z) &= \{u_x \ u_y \ u_z\}^T \\ \boldsymbol{\sigma} &= \{\sigma_{xx} \ \sigma_{yy} \ \sigma_{zz} \ \sigma_{xz} \ \sigma_{yz} \ \sigma_{xy}\}^T \\ \boldsymbol{\varepsilon} &= \{\varepsilon_{xx} \ \varepsilon_{yy} \ \varepsilon_{zz} \ \varepsilon_{xz} \ \varepsilon_{yz} \ \varepsilon_{xy}\}^T\end{aligned}\tag{1}$$

Under the assumption of small displacements and rotations, the geometrical relations between the strains and the displacements can be expressed in the following matrix forms:

$$\boldsymbol{\varepsilon} = \mathbf{D} \mathbf{u}\tag{2}$$

where \mathbf{D} is the linear differential operators defined as:

$$\mathbf{D} = \begin{bmatrix} \partial_x & 0 & 0 \\ 0 & \partial_y & 0 \\ 0 & 0 & \partial_z \\ \partial_z & 0 & \partial_x \\ 0 & \partial_z & \partial_y \\ \partial_y & \partial_x & 0 \end{bmatrix},\tag{3}$$

where $\partial_x = \frac{\partial(\cdot)}{\partial x}$, $\partial_y = \frac{\partial(\cdot)}{\partial y}$, and $\partial_z = \frac{\partial(\cdot)}{\partial z}$ are partial derivative operators.

According to the Hook's law, the stress-strain relationship is formulated as:

$$\boldsymbol{\sigma} = \mathbf{C} \boldsymbol{\varepsilon}\tag{4}$$

For the isotropic material, the matrix \mathbf{C} is

$$\mathbf{C} = \begin{bmatrix} \lambda + 2G & \lambda & \lambda & 0 & 0 & 0 \\ \lambda & \lambda + 2G & \lambda & 0 & 0 & 0 \\ \lambda & \lambda & \lambda + 2G & 0 & 0 & 0 \\ 0 & 0 & 0 & G & 0 & 0 \\ 0 & 0 & 0 & 0 & G & 0 \\ 0 & 0 & 0 & 0 & 0 & G \end{bmatrix}\tag{5}$$

where G and λ are the Lamé's parameters related to the properties of isotropic material, and one can use $G = E/(2(1 + \nu))$ and $\lambda = \nu E/((1 + \nu)(1 - 2\nu))$ in case of Poisson's ratio and Young's modulus [37].

3 Carrera Unified Formulation

Based on the CUF, the three-dimensional displacement field of the beam structures is formulated as [42]:

$$\mathbf{u}(x, y, z; t) = F_\tau(x, z) \mathbf{u}_\tau(y; t), \quad \tau = 0, 1, \dots, N,\tag{6}$$

where F_τ is the set of cross-section functions and \mathbf{u}_τ is the generalized displacement vector. Therefore, the expansions of any order could be selected over the beam cross-section that provides us with a great advantage of implementing different structural theories. Some examples in the literature are represented by orthogonal polynomials and trigonometric functions, see [43, 44]. In this research, Taylor expansions (TE) and Lagrange expansions (LE) are used as cross-section functions to model the beam structure.

By using polynomial expansion of the kind $x^m z^n$ as cross-section function F_τ , the TE models are formulated. Note that m and n are positive integers, and the order of TE model (N) refers to the structural theory of the beam which is defined as a user input. For example, in the linear case of $N = 1$, the displacement field is:

$$\begin{aligned} u_x(x, y, z; t) &= u_{x1}(y; t) + xu_{x2}(y; t) + zu_{x3}(y; t) \\ u_y(x, y, z; t) &= u_{y1}(y; t) + xu_{y2}(y; t) + zu_{y3}(y; t) \\ u_z(x, y, z; t) &= u_{z1}(y; t) + xu_{z2}(y; t) + zu_{z3}(y; t) \end{aligned} \quad (7)$$

The classical beam theories such as Euler–Bernoulli beam theory (EBBT) and Timoshenko beam theory (TBT) can be obtained as particular cases of linear TE [42].

LE have been demonstrated to be very efficient for several applications such as aerospace and civil structures [45, 46, 47, 48, 49]. For the LE models, the unknown variables are pure displacements. In this research paper, different numbers of nine-nodes Lagrange polynomials (L9) are adopted for the expansion function over the cross-section. The displacement field evaluated through one L9 polynomial is quadratic and reads:

$$\begin{aligned} u_x(x, y, z; t) &= F_1(x, z)u_{x1}(y; t) + F_2(x, z)u_{x2}(y; t) + \dots + F_9(x, z)u_{x9}(y; t) \\ u_y(x, y, z; t) &= F_1(x, z)u_{y1}(y; t) + F_2(x, z)u_{y2}(y; t) + \dots + F_9(x, z)u_{y9}(y; t) \\ u_z(x, y, z; t) &= F_1(x, z)u_{z1}(y; t) + F_2(x, z)u_{z2}(y; t) + \dots + F_9(x, z)u_{z9}(y; t) \end{aligned} \quad (8)$$

where u_{x1}, \dots, u_{z9} are the displacements of the points of the cross-sectional elements and F_1, \dots, F_9 are functions of the cross-sectional coordinates and represent the first 9 Lagrange polynomials of order 3 [41]. Interested readers are referred to the book by Carrera et al. for more information about the beam models with Lagrange expansions [42].

As an example of the mentioned expansion functions over the beam cross-section, a straight beam subjected to the bending around the z axis can be assumed. The deformed configuration is shown in Fig.1 according to the TE (order $N=1$, particular case Timoshenko beam) and LE (9 Lagrange points) models. As can be seen in this figure, for the case of linear TE ($N=1$), u_{x1} , u_{y1} , and u_{z1} are the beam axis displacements, and the other unknowns u_{x2} , u_{y2} , u_{z2} , u_{x3} , u_{y3} , and u_{z3} are rotations with respect to the axes. On the other hand, For the LE, the unknowns are the displacements of the points of the cross-sectional elements u_{x1}, \dots, u_{z9} .

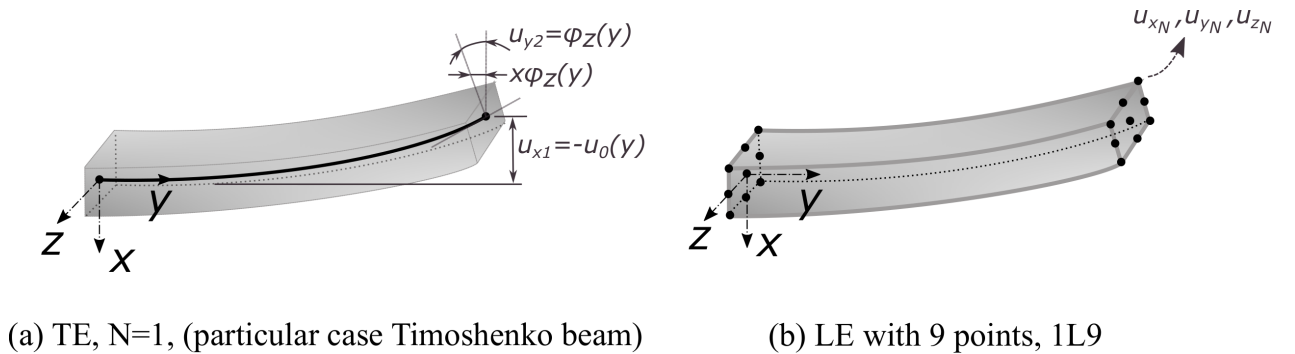


Figure 1: Schematic view of a beam bent around z axis based on the different expansion functions over the cross-section

3.1 Finite element approximation

By using the FE approximation, the displacement vector \mathbf{u}_τ based on the nodal parameters $\mathbf{u}_{\tau i}$ and shape functions N_i is expressed as:

$$\mathbf{u}_\tau(y; t) = N_i(y) \mathbf{u}_{\tau i}(t), \quad i = 1, 2, \dots, p+1, \quad (9)$$

where N_i is the i -th shape function and p is related to the order of the shape functions. More information about the Lagrange polynomials and shape functions can be found in [50]. By using the finite element approximation and the CUF, the displacement field can be defined as:

$$\mathbf{u}(x, y, z; t) = N_i(y) F_\tau(x, z) \mathbf{u}_{\tau i}(t) \quad (10)$$

Based on the Principle of Virtual Displacements (PVD), the equations of motion can be expressed as:

$$\delta L_{\text{int}} + \delta L_{\text{ine}} = \delta L_{\text{ext}} \quad (11)$$

where L_{int} , L_{ine} , and L_{ext} represent the strain energy, work of the inertial loadings, and the work of external loadings, respectively. For the free vibration analysis around trivial equilibrium states, the work of external loadings is zero, therefore:

$$\delta L_{\text{int}} + \delta L_{\text{ine}} = 0 \quad (12)$$

According to the CUF as discussed in the previous section, the following equations are obtained for the virtual variations of strain energy and the inertial work.

$$\begin{aligned} \delta L_{\text{int}} &= \int_V \delta \boldsymbol{\varepsilon}^T \boldsymbol{\sigma} dV = \delta \mathbf{u}_{sj}^T \left(\int_V F_s(x, z) N_j(y) \mathbf{D}^T \mathbf{C} \mathbf{D} N_i(y) F_\tau(x, z) dV \right) \mathbf{u}_{\tau i} = \delta \mathbf{u}_{sj}^T \mathbf{K}^{ij\tau s} \mathbf{u}_{\tau i} \\ \delta L_{\text{ine}} &= \int_V \delta \mathbf{u}^T \rho \ddot{\mathbf{u}} dV = \delta \mathbf{u}_{sj}^T \left(\int_V F_s(x, z) N_j(y) \rho N_i(y) F_\tau(x, z) dV \right) \ddot{\mathbf{u}}_{\tau i} = \delta \mathbf{u}_{sj}^T \mathbf{M}^{ij\tau s} \ddot{\mathbf{u}}_{\tau i} \end{aligned} \quad (13)$$

where $\mathbf{K}^{ij\tau s}$ and $\mathbf{M}^{ij\tau s}$ are the Fundamental Nuclei (FN) of the stiffness and mass matrices. These are 3*3 matrices based on the unified formulations for a given i, j pair, and independent of the order of the structure model with a fixed form. The global matrices are obtained by considering all the combinations of the indices i, j, τ , and s . More details about the fundamental nucleus formulation and their explicit forms can be found in [42, 51]. Interested readers are referred to [35] for the detailed procedure of the eigenvalue problem to evaluate the modal shapes and natural frequencies.

4 Numerical results

In this section, numerical results are presented for different thin-walled open cross-section beams. First, the vibration modes of these beams are investigated with a focus on the cross-sectional deformations. Then the corresponding natural frequencies are reported and compared with the numerical and experimental results from the literature. In addition, the results of linear buckling analysis are presented for different open cross-section beams. By using the proposed efficient CUF-1D models and the available literature, a comprehensive study is conducted in order to investigate the effect of compressive loads on the frequencies of the beams.

4.1 Beam 1- cruciform beam

The first beam example is a cruciform cross-section beam with the length of 670 mm [25]. The beam is doubly clamped, and all the translations and rotations are restrained for the bottom and top edges of the beam cross-section except for the vertical displacements of the top edge along the beam axis (y direction). The schematic view of the cruciform beam is shown in Fig. 2. Note that all the dimensions in this figure are in millimeters (mm). As shown in this figure, the thickness of

the beam cross-section is 1.1 mm. The isotropic material properties of Table 1 are considered for this cruciform beam.

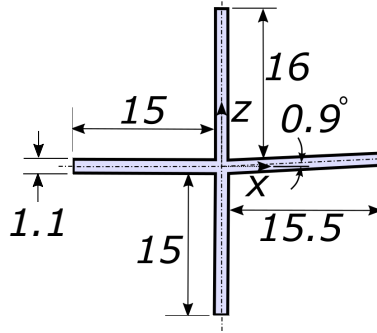


Figure 2: Schematic view of the cruciform beam

Table 1: Isotropic material properties of the cruciform beam

Material property	Value
Young's modulus	$E = 70 \text{ GPa}$
Poisson's ratio	$\nu = 0.3$
Density	$\rho = 2600 \frac{\text{Kg}}{\text{m}^3}$

The first ten vibration mode shapes of the cruciform beam based on the model with 105 Lagrange points and 20B4 elements are illustrated in Table. 2. As can be seen in this table, the second, third, seventh, and eighth bending modes occur in the 264.15, 270.47, 712.20, and 728.88 Hz, respectively. The middle cross-sectional view of the first ten vibration mode shapes in the cruciform beam based on the model with 117 Lagrange points and 20B4 elements is shown in Table. 3. The effect of cross-sectional deformations should be highlighted for this open cross-section beam. Therefore, the selection of structural theories capable of accurate detection of these cross-sectional deformations is necessary. The first ten buckling modes and the corresponding critical axial displacements of the cruciform beam based on the model with 105 Lagrange points and 20B4 elements are displayed in Fig. 4. As evident from the table, the first buckling and vibration modes are similar.

The first ten natural frequencies of the unloaded cruciform beam based on the CUF-1D models and the literature are compared in Table 5. In this table, the numbers of beam elements, Lagrange points, and DOFs are presented for different CUF-1D models using the Taylor and Lagrange expansions. In addition, the values of natural frequencies from the available literature [25] by using experimental methods and three numerical methods based on the thin shell, thick shell, and solid brick elements are reported in Table 5. The results show that the natural frequencies obtained by the CUF-1D with 20B4 and at least 57 Lagrange points correlate well with the literature results. This shows the capability of cost-effective CUF-1D models to detect vibration modes and the cross-sectional deformations in this open cross-section thin-walled beam. It should be noted that all the experimental natural frequencies of Ref. [25] are obtained by the PZT pickups, except for the first value in the parenthesis, which refers to the fundamental frequency obtained by the laser sensor.

Table 2: The first ten vibration mode shapes of the cruciform beam based on the model with 105 Lagrange points and 20B4 elements

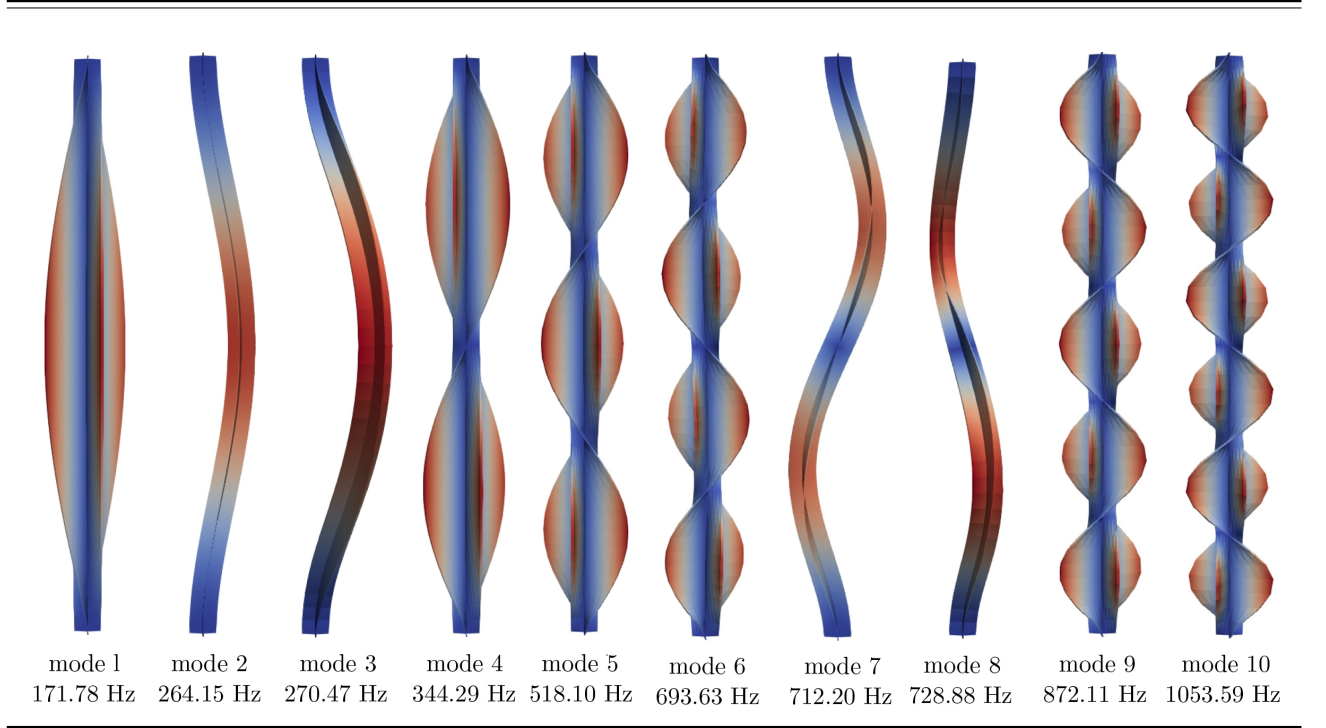


Table 3: Middle cross-sectional view of the first ten vibration mode shapes in the cruciform beam based on the model with 105 Lagrange points and 20B4 elements

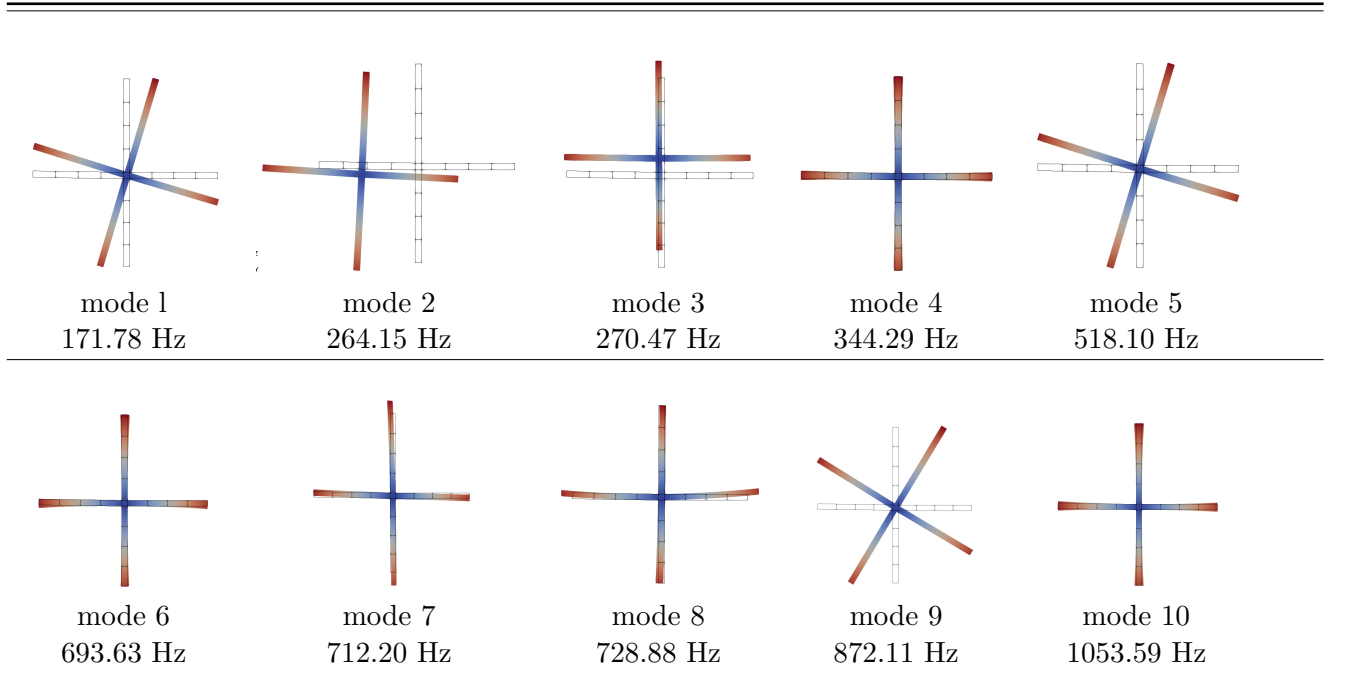


Table 4: The first ten buckling modes and the corresponding critical axial displacements of the cruciform beam based on the model with 105 Lagrange points and 20B4 elements

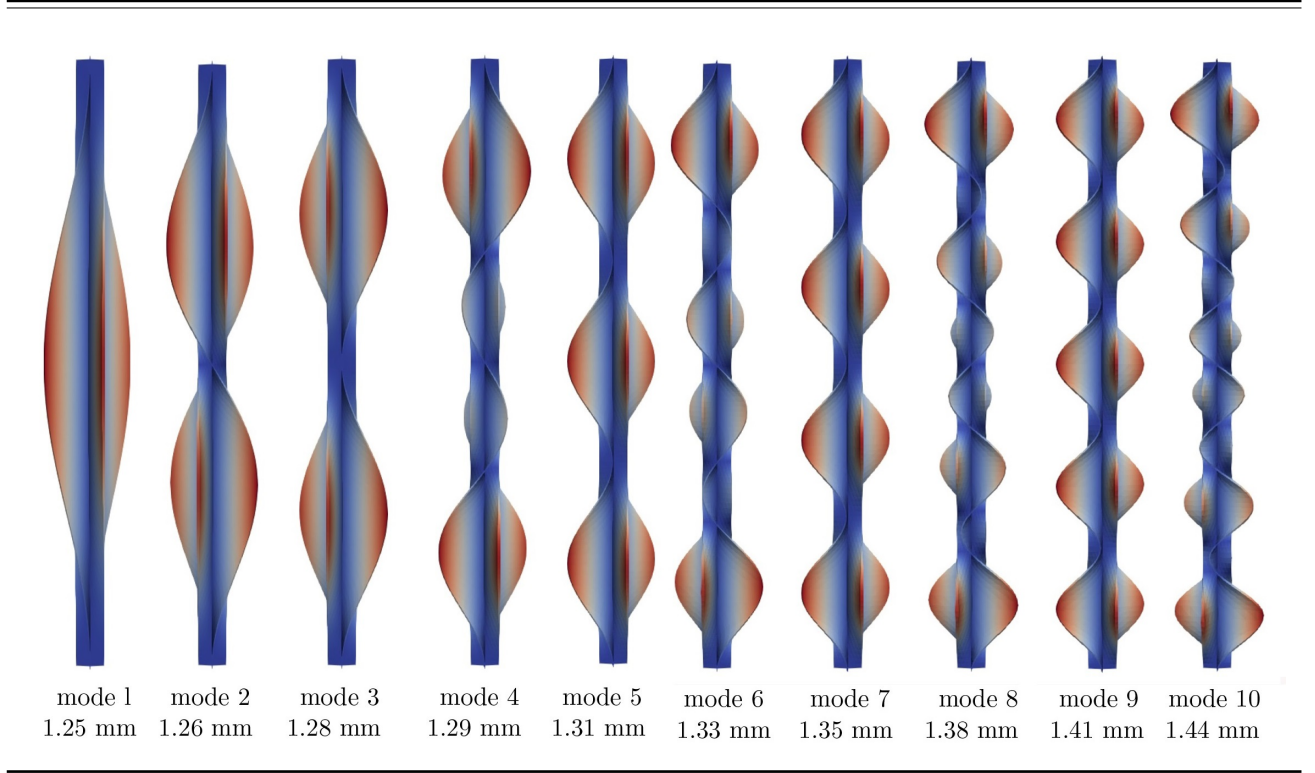


Table 5: Evaluation of the first ten natural frequencies of the unloaded cruciform beam based on the CUF-1D models and the literature

Model	Beam elements	Lag. Points	DOF	Buck. load (KN)	Natural Frequency (Hz)								
					Mode 1	Mode 2	Mode 3	Mode 4	Mode 5	Mode 6	Mode 7	Mode 8	Mode 9
Lagrange(25L9)	5B4	153	7344	5.07	175.77	267.19	273.56	352.38	531.41	714.84	721.24	737.90	915.89
Lagrange(25L9)	10B4	153	14229	8.45	172.27	265.07	271.40	345.26	519.57	695.75	714.49	731.24	875.24
Taylor order 1	20B4	-	549	8.94	265.09	271.68	724.47	742.17	1437.72	1404.21	2288.81	2341.88	2401.44
Taylor order 2	20B4	-	1098	9.05	273.12	266.51	728.32	746.05	1411.60	1445.13	2300.75	2353.79	2400.70
Taylor order 10	20B4	-	12078	8.82	264.20	270.96	326.25	648.65	717.66	733.41	970.92	1288.23	1367.62
Lagrange(5L9)	20B4	33	6039	8.81	176.13	264.35	270.66	353.01	531.17	730.94	715.03	710.24	893.86
Lagrange(9L9)	20B4	57	10431	8.76	173.65	264.22	270.53	348.04	523.73	701.02	712.89	729.46	881.52
Lagrange(17L9)	20B4	105	19215	8.68	171.78	264.16	270.47	344.30	518.11	693.63	712.20	728.89	872.11
Lagrange(25L9)	20B4	153	27999	8.65	171.06	264.14	270.45	342.85	515.95	690.78	712.01	728.72	868.52
Thin shell [25]					165.54	278.43	284.99	331.75	499.22	668.52	749.31	766.7	840.35
Thick shell [25]					163.86	278.43	284.99	328.4	494.22	661.87	749.32	766.71	832.09
Solid brick [25]					160.91	270.75	281.59	329.69	484.58	676.69	749.29	765.76	816.26
Experiment [25]					161.87(160.92)	275.47	284.18	325.43	486.13	667.84	741.30	767.53	813.39

Regarding the reported values in Table 5 it should be outlined that many of the mode shapes based on different structural theories are not corresponding to each other. Therefore, the MAC analysis could be used in order to investigate the corresponding modes related to each theory. The MAC is defined as a scalar that represents the degree of consistency between two distinct modal vectors in such a way that the values change from 0 to 1. The MAC value of 0 represents no consistent correspondence of the models. The MAC is obtained according to the following equation [37, 52, 53, 54]:

$$MAC_{ij} = \frac{\left| \{\varphi_{A_i}\}^T \{\varphi_{B_j}\} \right|^2}{\{\varphi_{A_i}\}^T \{\varphi_{A_i}\} \{\varphi_{B_j}\} \{\varphi_{B_j}\}^T} \quad (14)$$

where φ_{A_i} is the i th eigenvector of model A, and φ_{B_j} is the j th eigenvector of model B.

By using the MAC analysis, the comparison of free vibration modes for the cruciform beams with 20B4 elements based on different structural theories versus the Lagrange model with 153 points is indicated in Fig. 3. As can be noticed from this figure, the number of corresponding modes for the classical models such as Taylor order 1 is less compared to the other Lagrange models. In fact, many modes are lost by classical beam theories, and instead, they show rigid cross-section modes that do not really exist. Four black squares in Fig. 3a are indicative of the correspondence of the Taylor modes 2, 3, 4, and 9 to the Lagrange modes of 3, 7, 8, and 1, respectively. These mode shapes are shown in Table 6 for the Taylor order 1 model and Lagrange model with 153 points. It is noteworthy to mention the fact that although some modes might be corresponding to each other according to the MAC analysis, the values of natural frequencies based on the two models might show higher discrepancies. For instance, the two torsional modes of Taylor mode 9 and Lagrange mode 1 in Table 6 are corresponded to each other, while the natural frequencies obtained by these two models are considerably different. The importance of the selection of structural theory capable of detecting the accurate eigenvalues and eigenvectors of the structural problem should be highlighted.

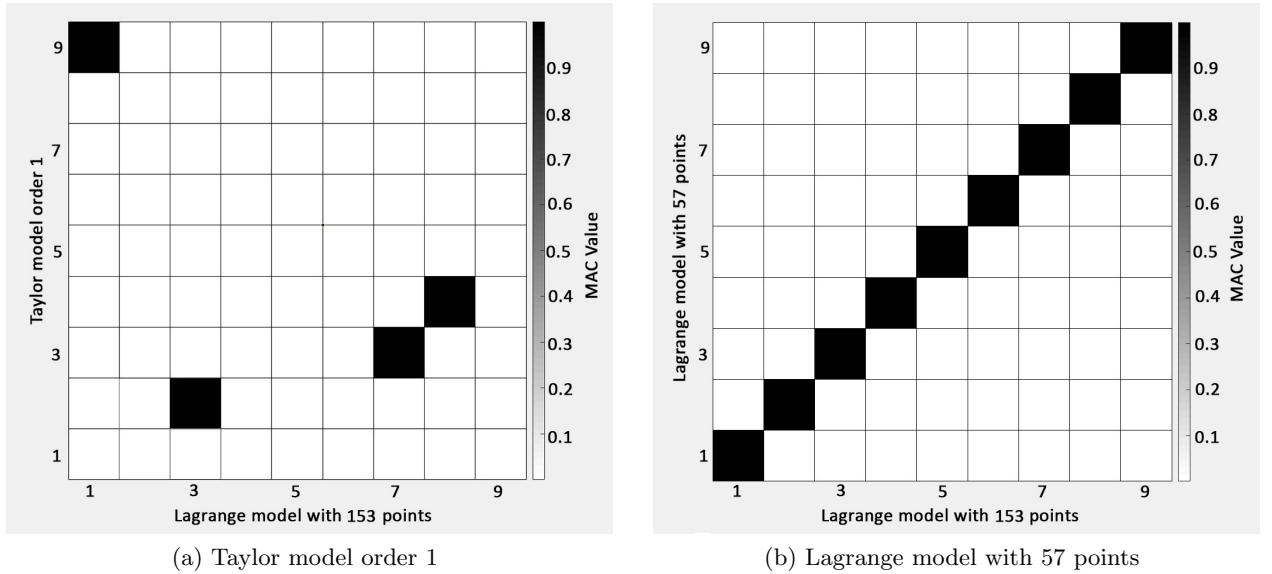
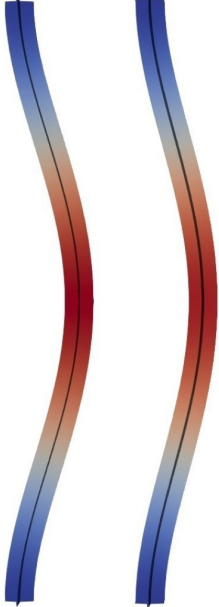
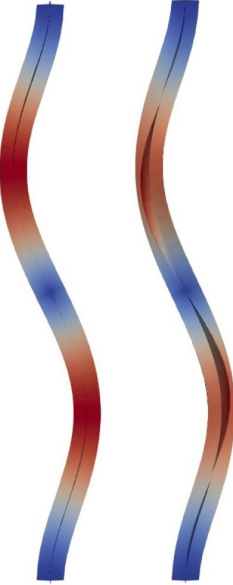

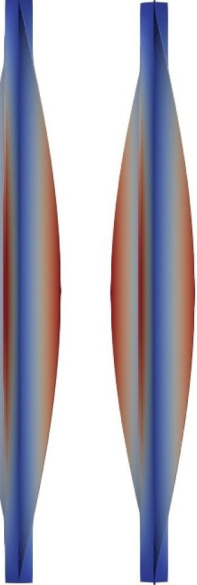


Figure 3: The comparison of free vibration modes using the MAC analysis for the cruciform beams with 20B4 elements based on different structural theories versus the Lagrange model with 153 points

Table 6: The corresponding vibration mode shapes of the cruciform beam obtained by the MAC analysis for the Taylor model order 1 and Lagrange model with 153 points (See Fig 3a)

Tay.2, Lag.3		Tay.3, Lag.7		Tay.4, Lag.8		Tay.9, Lag.1	
							
Taylor mode 2	Lagrange mode 3	Taylor mode 3	Lagrange mode 7	Taylor mode 4	Lagrange mode 8	Taylor mode 9	Lagrange mode 1
271.67 Hz	270.45 Hz	724.47 Hz	712.01 Hz	742.16 Hz	728.72 Hz	2401.43 Hz	171.06 Hz

The first five natural frequencies in the cruciform beam under progressive compressive loads based on the CUF model with 153 Lagrange points and Ref. [25] are compared in Table. 4. The plotted values of this table show that the natural frequencies decrease by the compressive loads because of the decrease in the stiffness of the beam structure. It is visible that the natural frequencies obtained by the efficient CUF-1D models proposed here are in good agreement with the experimental results obtained in Ref. [25]. The values of fundamental frequencies in the cruciform beam under progressive compressive loads based on the CUF-1D model with 153 Lagrange points and Ref. [25] are reported in Table 7 where the first two columns are devoted to the fundamental frequencies obtained by the Laser and PZT sensors for the experimental method.

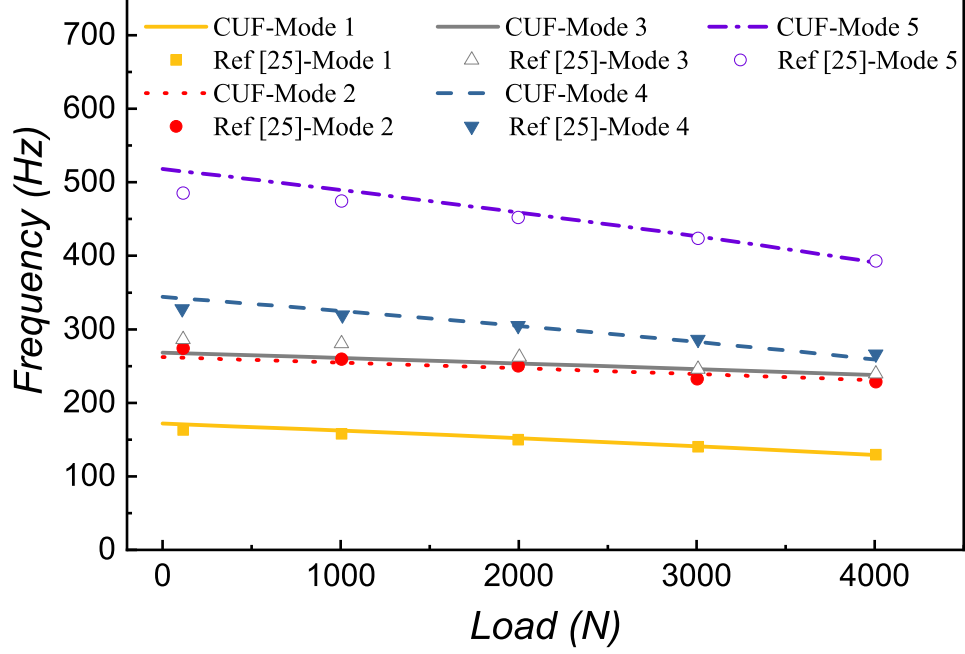
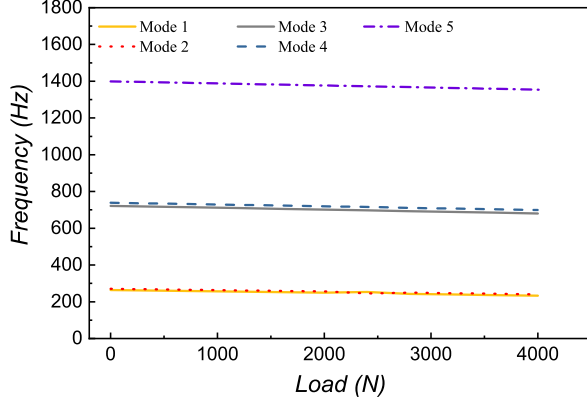


Figure 4: The comparison of the first five natural frequencies in the cruciform beam under progressive compressive loads based on the CUF model with 105 Lagrange points and Ref. [25]

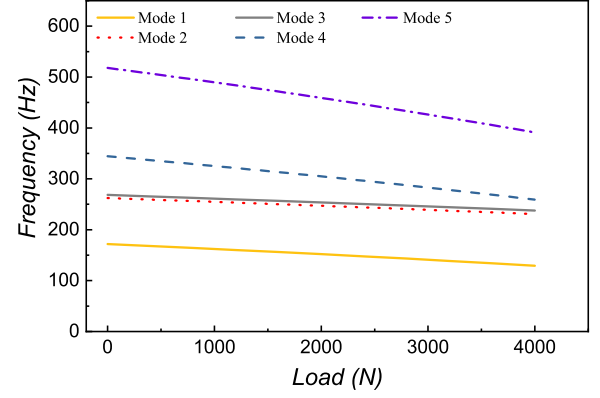
Table 7: Evaluation of fundamental frequencies in the cruciform beam under progressive compressive loads based on the CUF-1D model with 105 Lagrange points and the literature

Load (KN)	Frequency (Hz)-Laser [25]	Frequency (Hz)-PZT [25]	Frequency (Hz)-CUF 1D
0.00	161.73	161.87	171.78
0.24	156.88	159.12	171.08
0.49	154.08	156.42	168.27
1.00	150.04	151.69	162.55
1.41	146.60	149.22	157.95
2.02	142.44	145.42	151.10
2.46	139.60	142.33	146.16
2.98	135.94	138.24	140.32
3.43	132.33	134.61	135.27
3.95	130.96	131.33	129.43

The first five natural frequencies in the cruciform beam under progressive compressive loads based on the CUF model with 105 Lagrange points and Taylor model order 1 are compared in Fig. 5. As illustrated in this figure, the effect of compressive loads on the variations of natural frequencies is more evident by using the refined theories using Lagrange expansion. Furthermore, it should be noted that some modes are missed based on the classical models; for instance, the first torsional mode is not detected by the Taylor order 1 model.



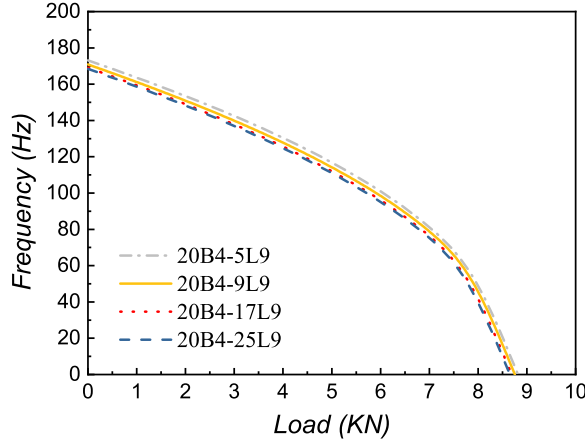
(a) Taylor model order 1



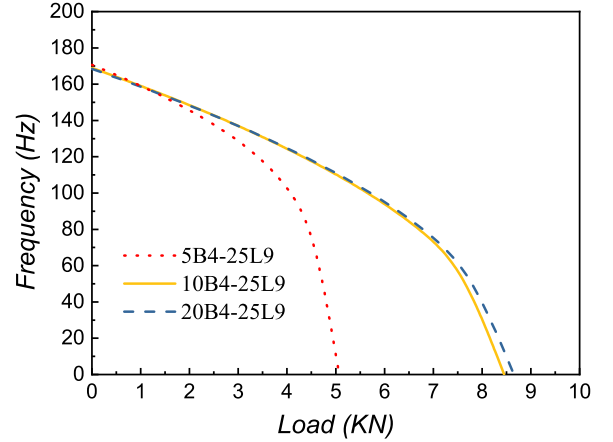
(b) Lagrange model with 105 points

Figure 5: The comparison of the first five natural frequencies in the cruciform beam under progressive compressive loads based on the Taylor model order 1 and CUF model with 105 Lagrange points

The effects of structural theory and FE discretization on the fundamental frequencies of the cruciform beam under progressive compressive loads are investigated in Fig. 6. In this figure, the values of the fundamental frequency are plotted versus the applied compressive loads. As can be seen in this figure, the convergence is achieved well by the presented Lagrange models except for the model with only 5 B4 elements. The Critical buckling loads and the fundamental frequencies versus the applied progressive compressive loads in the cruciform beam according to the Ref. [25] and the CUF-1D model are shown in Fig. 7. The CUF-1D results demonstrate that the critical buckling load and the variations of natural frequencies with the progressive loads correlate well with the available literature, and the proposed method can be used effectively in order to investigate the natural frequencies of loaded beams under compression.



(a) Theory approximations



(b) Mesh sized

Figure 6: The variations of fundamental frequencies in the cruciform beam under progressive compressive loads based on the different CUF-1D models(a) effect of the structural theory (b) effect of FE discretization

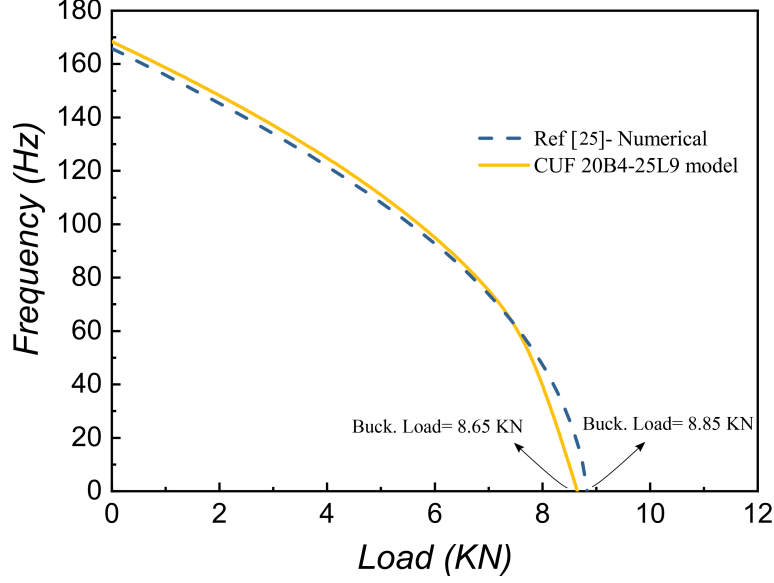


Figure 7: Critical buckling loads and the fundamental frequencies versus the applied progressive compressive loads in the cruciform beam according to the Ref. [25] and the CUF-1D model

4.2 Beam 2- thin cruciform beam

For comparison purposes, a thinner cruciform beam with a thickness of 0.2 mm is investigated. Similar to the previous beam, the length of the beam is 670 mm , and the boundary conditions are doubly clamped except for the vertical displacements of the top edge along the beam axis (y direction). The schematic view of the thin cruciform beam is shown in Fig. 8. Note that all the dimensions in this figure are in millimeters (mm). The isotropic material properties of Table 1 are also considered for this beam example.

The first ten vibration mode shapes of the thin cruciform beam based on the model with 105 Lagrange points and 20B4 elements are shown in Table. 8. Moreover, the middle cross-sectional view of the first ten vibration mode shapes in the thin cruciform beam based on the model with 105 Lagrange points and 20B4 elements are illustrated in Table 9. It should be outlined that, as evident from this Table, for the thin cruciform beam, the first eight modes are torsional, then two bending modes of number 8 and 9 occur in the 250.00 and 256.39 Hz frequencies, respectively. Comparing Tables 2 and 8, it can be observed that for this beam with thinner cross-section, the torsional modes with cross-sectional deformations occur before the other bending modes.

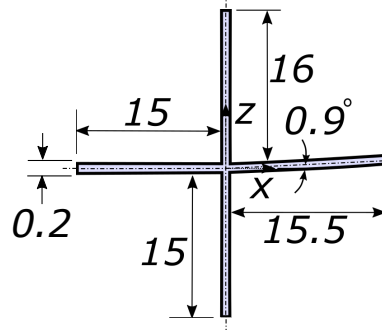


Figure 8: Schematic view of the thin cruciform beam

Table 8: The first ten vibration mode shapes of thin cruciform beam based on the model with 105 Lagrange points and 20B4 elements (See table 2 for comparison)

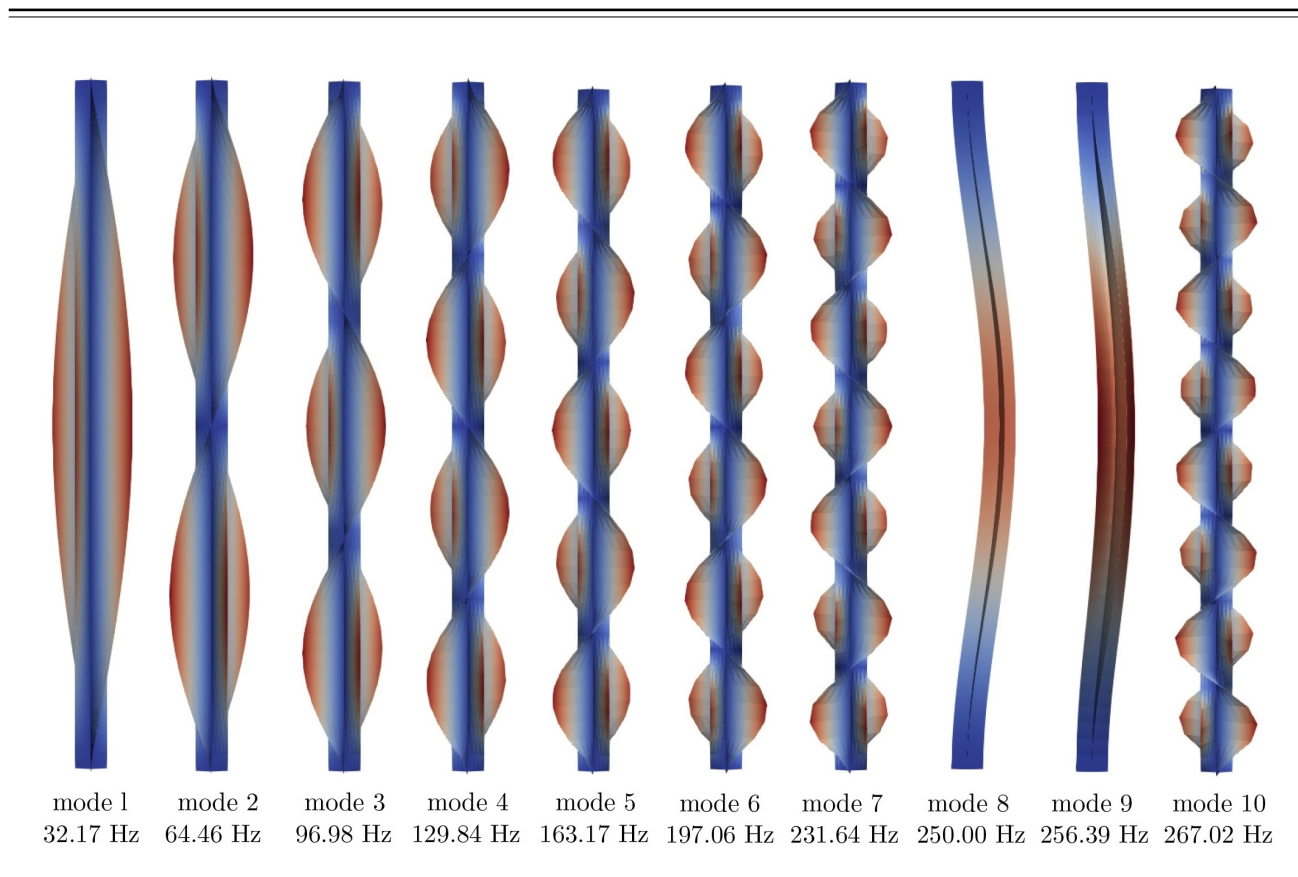
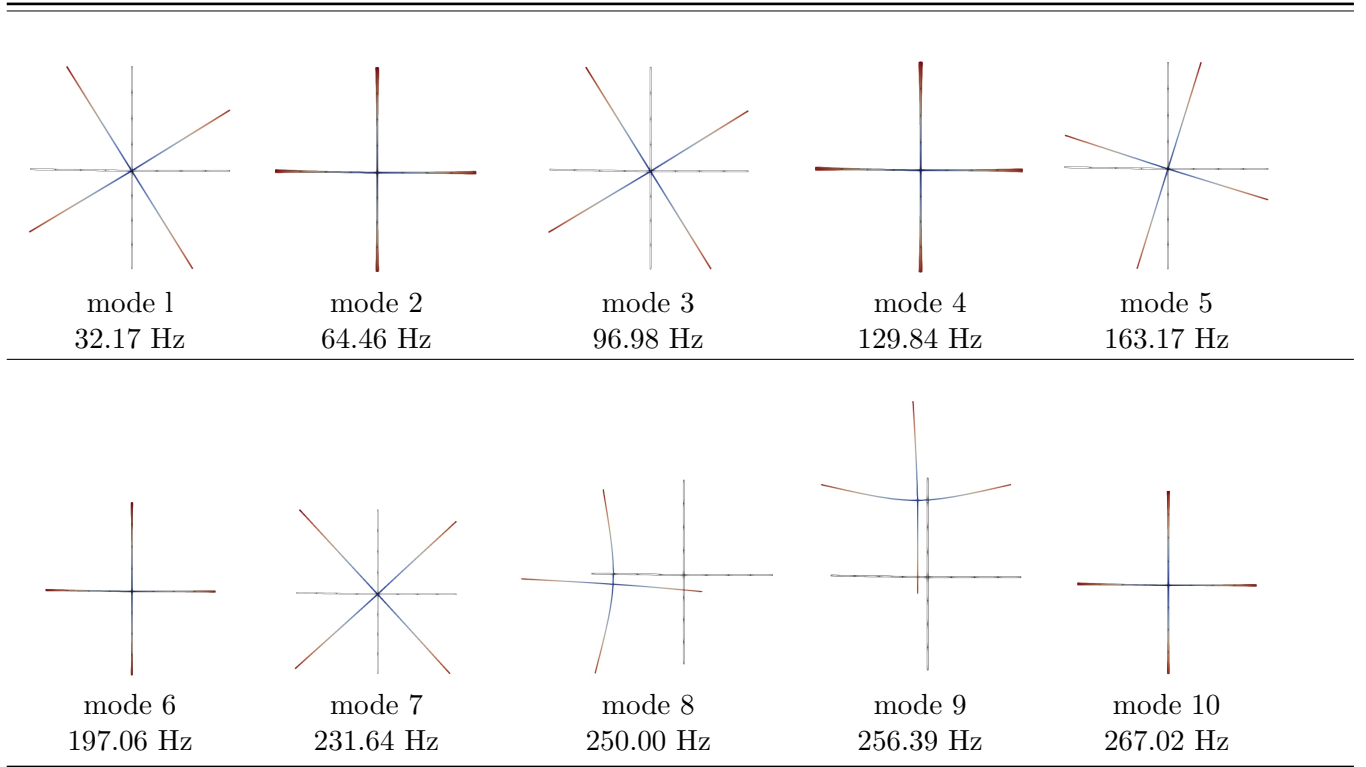


Table 9: Middle cross-sectional view of the first ten vibration mode shapes in the thin cruciform beam based on the model with 105 Lagrange points and 20B4 elements

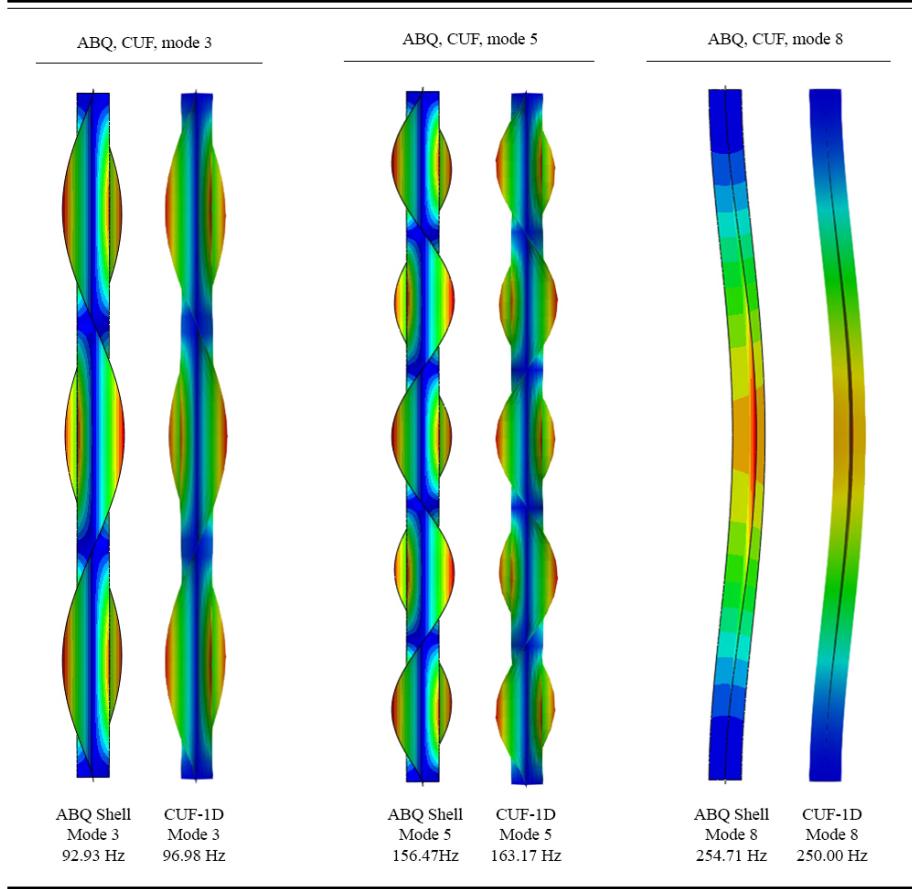


The first ten natural frequencies of the unloaded thin cruciform beam based on the CUF-1D Lagrange model and the thin ABQ shell model are compared in Table 10. In addition, the corresponding free vibration mode shapes are illustrated in Table 11. The results show that not only the mode shapes but also the natural frequencies obtained by the CUF-1D Lagrange model match well with the thin ABQ shell model. On the other hand, it is clear that CUF requires lower DOFs and computational costs in comparison with expensive shell models.

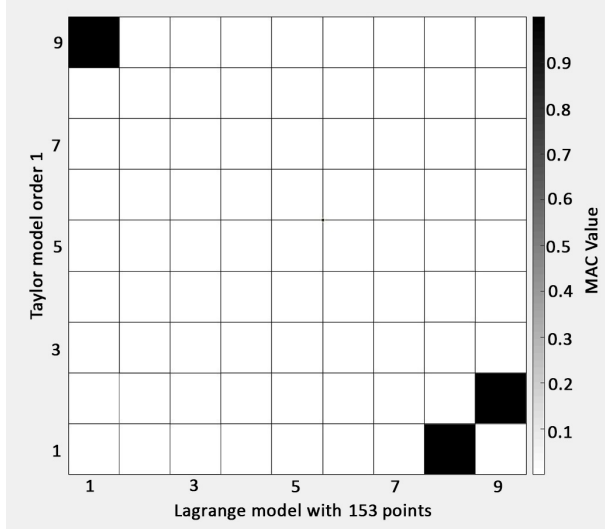
Table 10: Evaluation of the first ten natural frequencies of the unloaded thin cruciform beam based on the CUF-1D Lagrange model and the thin ABQ shell model

Model	No. of elements	Lag. Points	DOF	Natural Frequency (Hz)								
				Mode 1	Mode 2	Mode 3	Mode 4	Mode 5	Mode 6	Mode 7	Mode 8	Mode 9
CUF-1D (Lagrange)	20 B4	105	19215	32.17	64.46	96.98	129.84	163.17	197.06	231.64	250.00	256.39
Thin ABQ shell	1680 quadratic S8R	-	52396	30.82	61.76	92.93	124.47	156.47	189.05	222.32	254.71	261.08

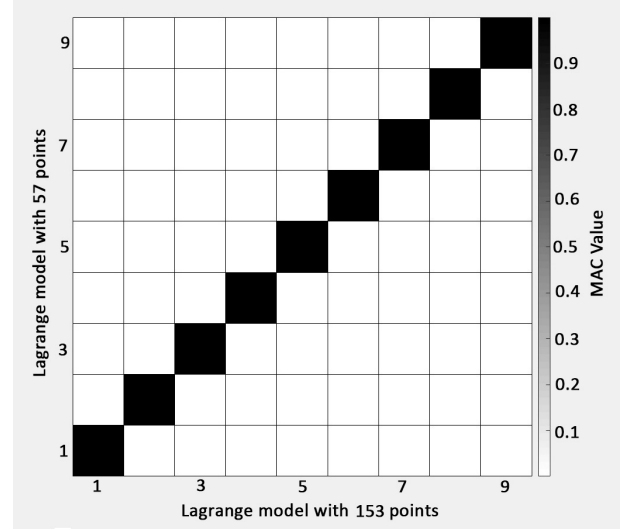
Table 11: The comparison of free vibration mode shapes of the thin cruciform beam based on the CUF-1D Lagrange model and the thin ABQ shell model



Similar to the previous beam example, the MAC analysis is used here in order to compare the free vibration modes of the thin cruciform beams with 20B4 elements based on different structural theories versus the Lagrange model with 153 points. As can be understood from Fig. 9, the number of corresponding modes for the classical models such as Taylor order 1 is less compared to the other Lagrange models. It is also noticed that for the case of the cruciform beam with a thinner cross-section, the adoption of refined theories is mandatory. The first five natural frequencies in the thin cruciform beam under progressive compressive loads based on the CUF model with 105 Lagrange points and Taylor model order 1 are compared in Fig. 10. As illustrated in this figure, the effect of compressive loads on the variations of natural frequencies is more evident by using the refined theories using Lagrange expansion. Moreover, one could notice that most of the first seven torsional modes are not detected by the classical theories.

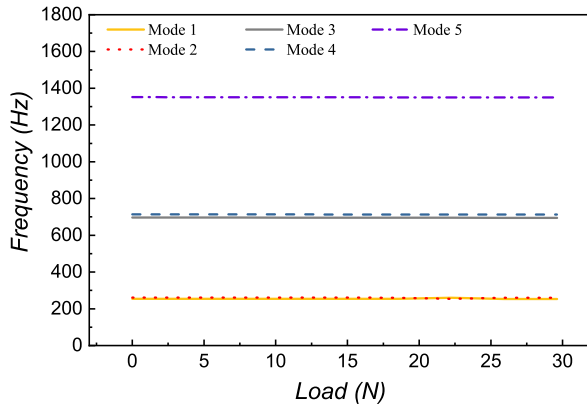


(a) Taylor model order 1

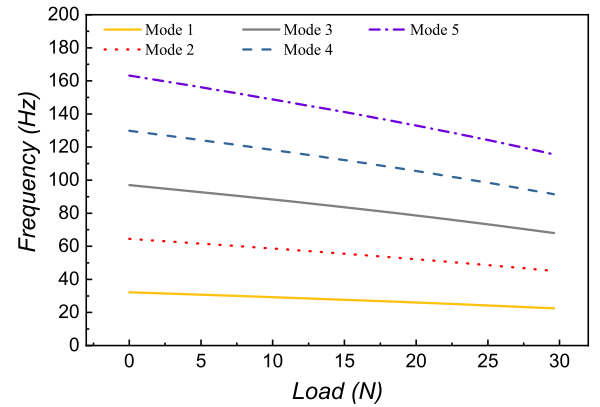


(b) Lagrange model with 57 points

Figure 9: The comparison of free vibration modes using the MAC analysis for the cruciform beams with 20B4 elements based on different structural theories versus the Lagrange model with 153 points



(a) Taylor model order 1



(b) Lagrange model with 105 points

Figure 10: The comparison of the first five natural frequencies in the thin cruciform beam under progressive compressive loads based on the Taylor model order 1 and CUF model with 105 Lagrange points

4.3 Beam 3- arbitrary cross-section

The third beam example is an arbitrary cross-section beam with a length of 950 mm [18]. The beam is doubly clamped, and all the translations and rotations are restrained for the bottom and top edges of the beam cross-section except for the vertical displacements of the top edge along the beam axis (y direction). The schematic view of the cruciform beam is shown in Fig. 11. Note that all the dimensions in this figure are in millimeters (mm). As shown in this figure, the thickness of the beam cross-section is 1.2 mm in the flanges and 1.4 mm in the webs. The isotropic material properties of Table 12 are considered for this beam.

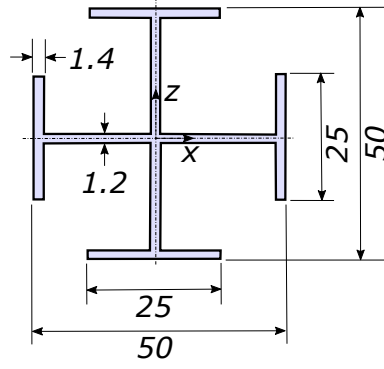


Figure 11: Schematic view of the beam 3- arbitrary cross-section

Table 12: Isotropic material properties of the beam 3- arbitrary cross-section

Material property	Value
Young's modulus	$E = 69 \text{ GPa}$
Poisson's ratio	$\nu = 0.3$
Density	$\rho = 2600 \frac{\text{Kg}}{\text{m}^3}$

The first ten vibration mode shapes of the beam 3- arbitrary cross-section based on the model with 129 Lagrange points and 20B4 elements are indicated in Table. 13. The middle cross-sectional view of the first ten vibration mode shapes in this beam based on the model with 129 Lagrange points and 20B4 elements is shown in Table. 14. This table confirms the necessity of selecting structural theories capable of detecting the cross-sectional deformations accurately. The first ten buckling modes and the corresponding critical axial displacements of the beam 3- arbitrary cross-section based on the model with 129 Lagrange points and 20B4 elements are displayed in Table. 15. As evident from this table, the first buckling and vibration modes are similar.

The first five natural frequencies in the beam 3- arbitrary cross-section under progressive compressive loads based on the CUF model with 129 Lagrange points and Ref. [18] are compared in Fig. 12. The plotted values of this figure confirm that the natural frequencies decrease by the compressive loads and their values correlate well with the experimental results obtained in Ref. [18]. The values of the first three frequencies in the beam 3- arbitrary cross-section under progressive compressive loads based on the CUF-1D model with 129 Lagrange points and Ref. [18] are reported in Table 16.

Table 13: The first ten vibration mode shapes of the beam 3- arbitrary cross-section based on the model with 129 Lagrange points and 20B4 elements

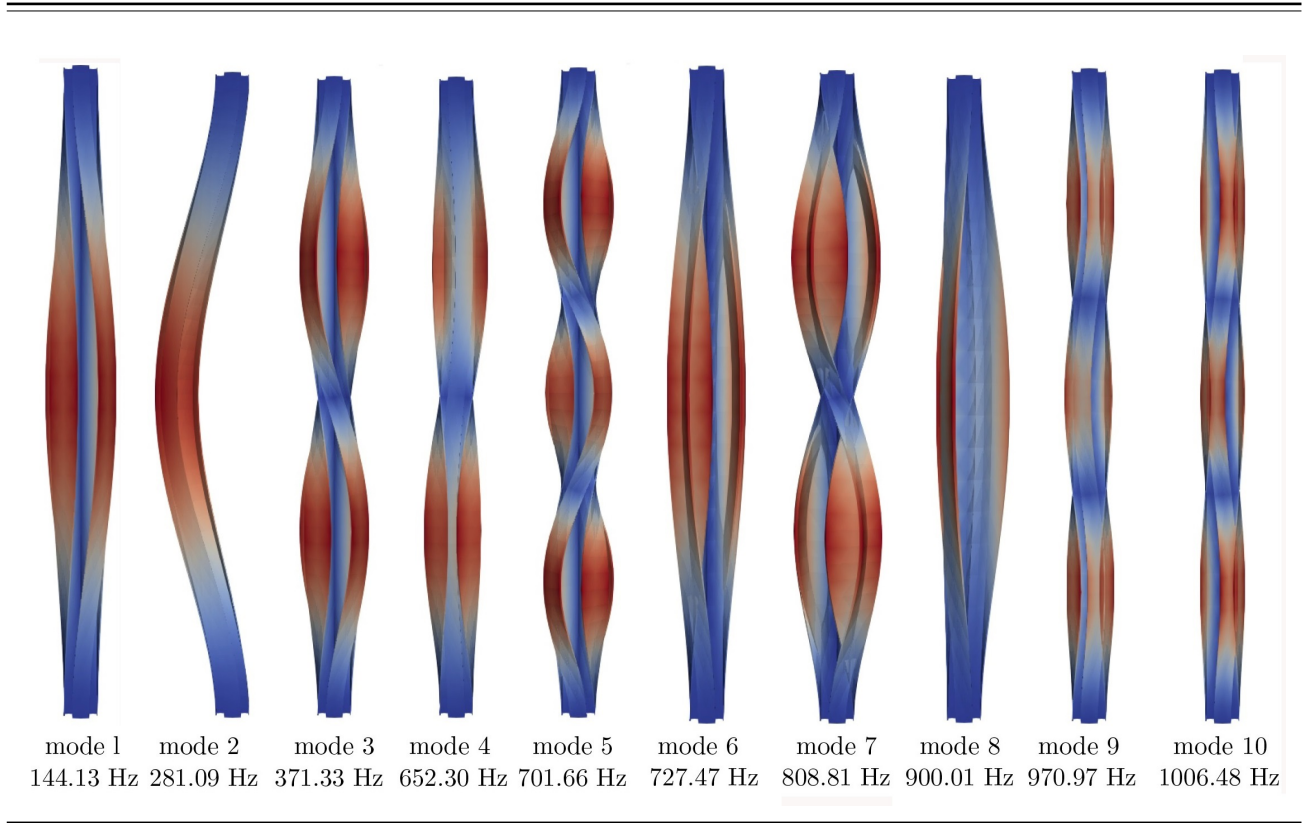


Table 14: Middle cross-sectional view of the first ten vibration mode shapes in the beam 3- arbitrary cross-section based on the model with 129 Lagrange points and 20B4 elements

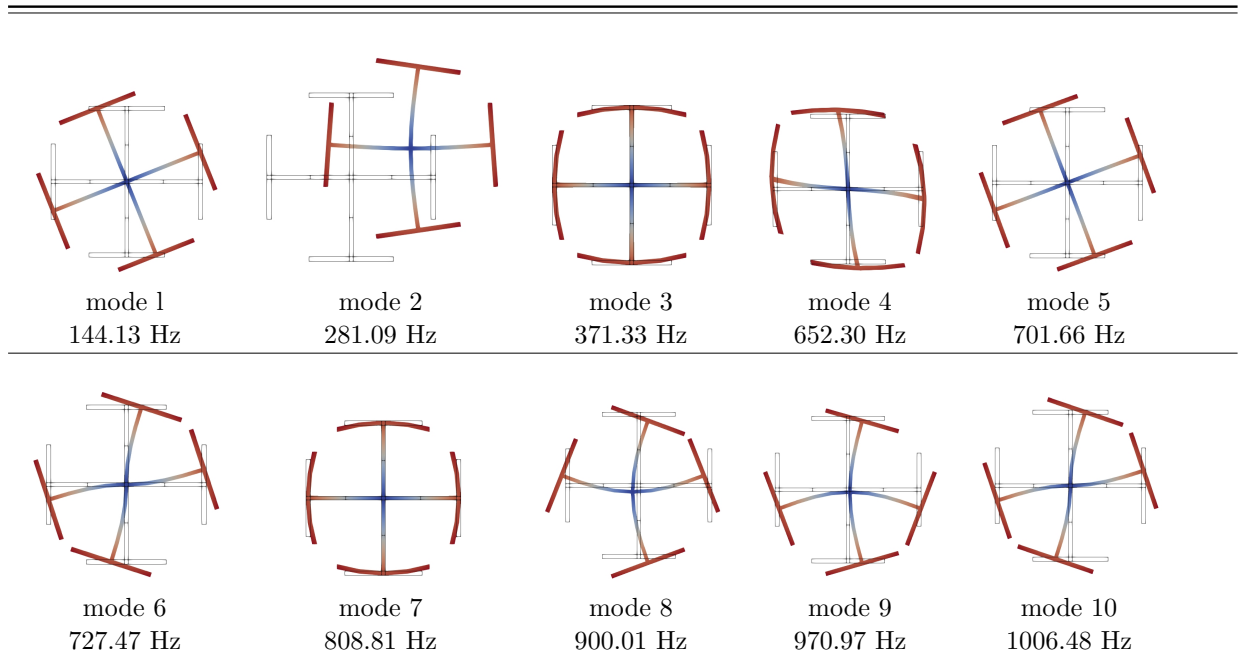


Table 15: The first ten buckling modes and the corresponding critical axial displacements of the beam 3- arbitrary cross-section based on the model with 129 Lagrange points and 20B4 elements

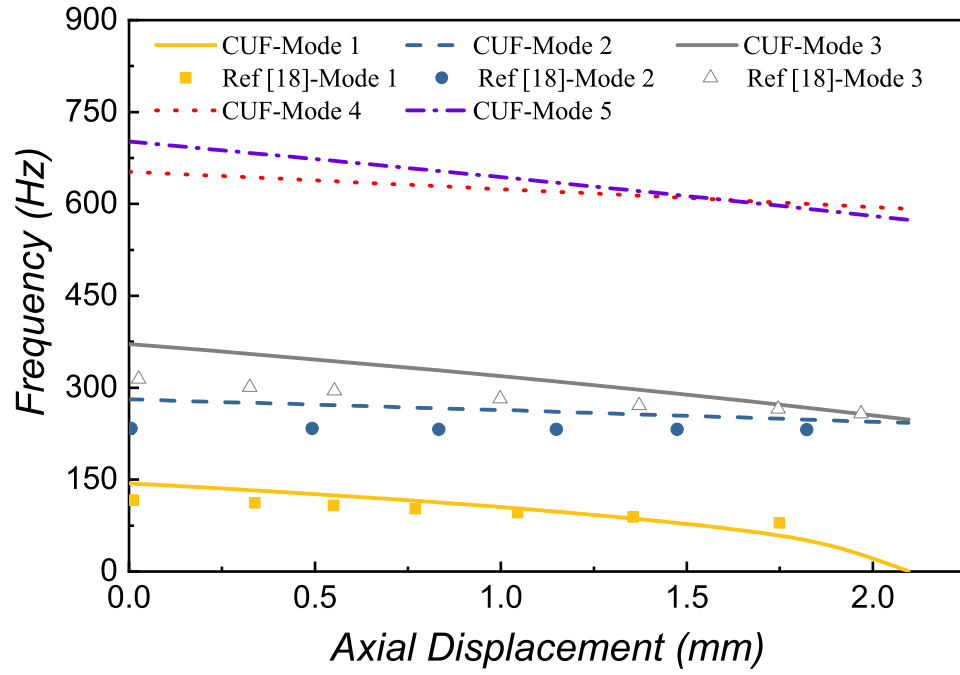
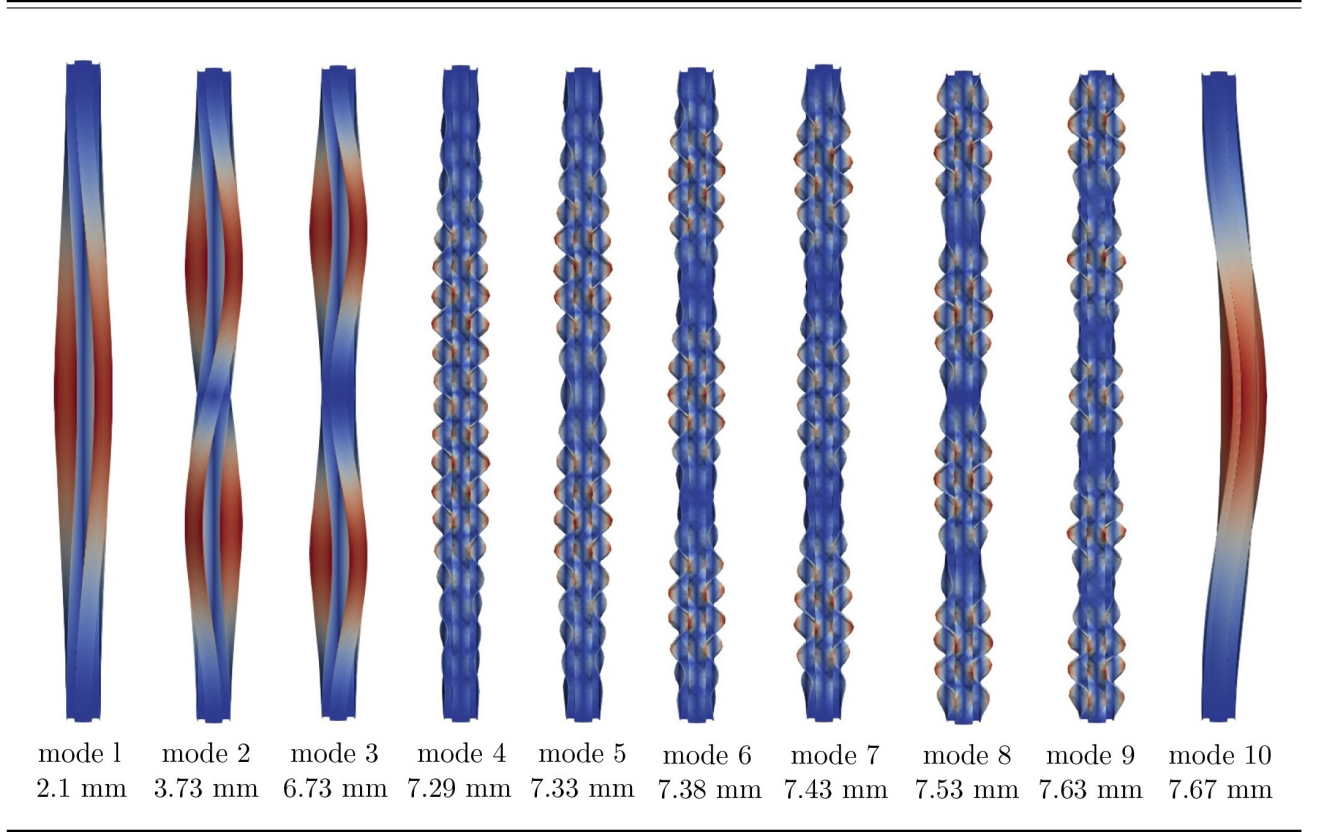


Figure 12: The comparison of the first five natural frequencies of the beam 3- arbitrary cross-section under progressive compressive loads based on the CUF model with 129 Lagrange points and Ref. [18]

Table 16: The variations of frequencies versus the applied axial displacements in the beam 3- arbitrary cross-section under progressive compressive loads based on the CUF-1D models and Ref. [18]

Axial Displacement (mm)	Frequency (Hz)- CUF			Frequency (Hz)-Ref. [18]		
	Mode 1	Mode 2	Mode 3	Mode 1	Mode 2	Mode 3
0.25	134.91	275.74	359.76	113.61	233.14	302.96
0.50	125.44	272.19	346.75	108.88	233.14	295.86
0.75	115.98	267.46	332.54	102.96	231.95	288.76
1.00	104.14	262.72	318.34	97.04	231.95	281.66
1.25	92.31	259.17	304.14	91.12	231.95	273.37
1.50	76.92	253.25	288.76	85.21	231.95	268.64
1.75	60.36	249.70	272.19	79.29	231.95	265.09

4.4 Beam 4- arbitrary cross-section

The final beam example is an arbitrary cross-section beam with a length of 9 m [28]. The beam is doubly clamped, and all the translations and rotations are restrained for the bottom and top edges of the beam cross-section except for the vertical displacements of the top edge along the beam axis (y direction). The schematic view of the cruciform beam is shown in Fig. 13. Note that all the dimensions in this figure are in millimeters (mm). As shown in this figure, the thickness of the beam cross-section is 4 mm. The isotropic material properties of Table 17 are considered for this beam.

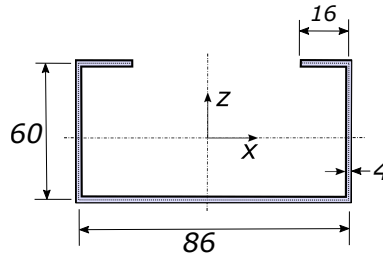


Figure 13: Schematic view of the beam 4- arbitrary cross-section

Table 17: Isotropic material properties of the beam 4- arbitrary cross-section

Material property	Value
Young's modulus	$E = 210 \text{ GPa}$
Poisson's ratio	$\nu = 0.3$
Density	$\rho = 7850 \frac{\text{Kg}}{\text{m}^3}$

The first ten vibration mode shapes of the beam 4- arbitrary cross-section based on the model with 117 Lagrange points and 20B4 elements are indicated in Table. 18. The middle cross-sectional view of the first ten vibration mode shapes in this beam based on the model with 117 Lagrange points and 20B4 elements is shown in Table. 19. The fourth mode shape shows in-plane stretching of the lateral walls, which is not a common result, considering the low frequency. This can be explained by the complex geometry of the cross-section and highlights the need for the adoption of refined models. The first five natural frequencies in the beam 4- arbitrary cross-section under progressive compressive loads based on the CUF model with 117 Lagrange points and the numerical results of the literature are compared in Fig. 14. The results of this figure confirm the fact that the obtained results by the proposed efficient CUF-1D models correlate well with the shell models in Ref. [28] which are more expensive in terms of computational cost. The values of the first three frequencies

in the beam 4- arbitrary cross-section under progressive compressive loads based on the CUF-1D model with 117 Lagrange points and Ref. [28] are reported in Table 20.

Table 18: The first ten vibration mode shapes of the beam 4- arbitrary cross-section based on the model with 117 Lagrange points and 20B4 elements

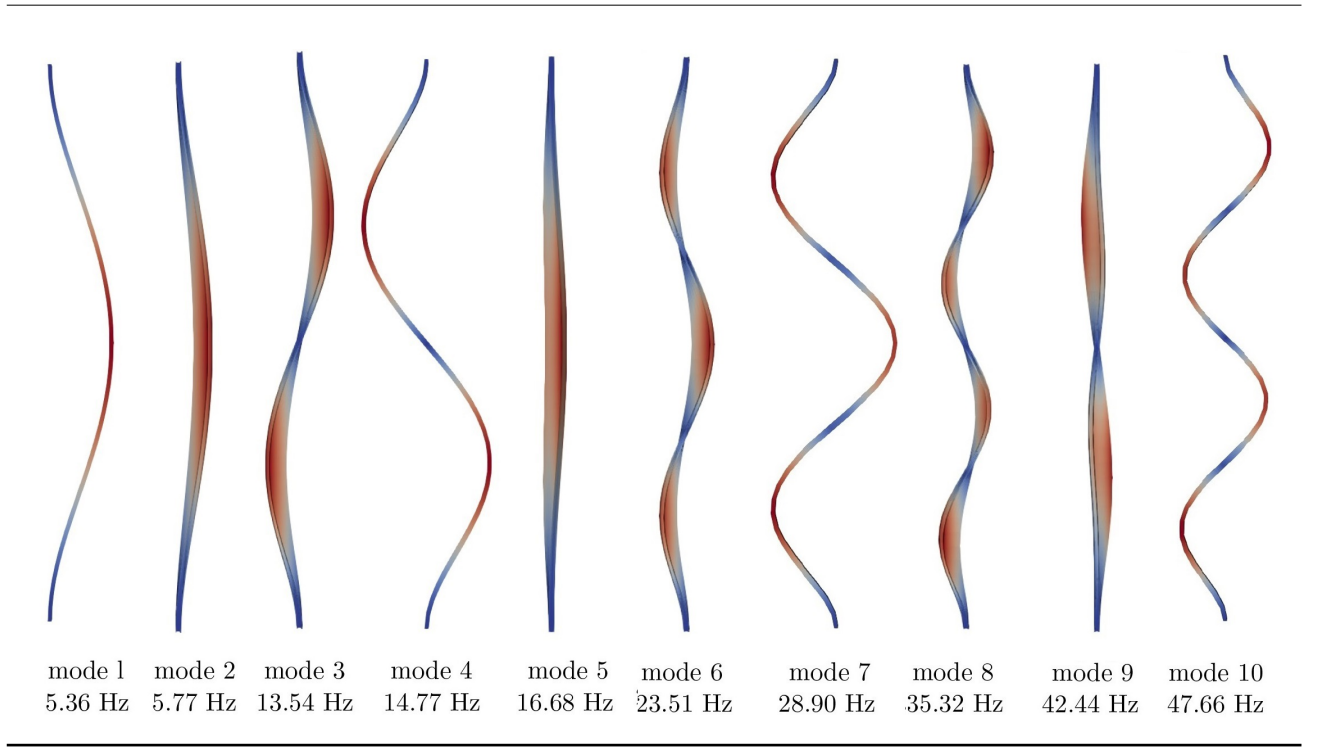
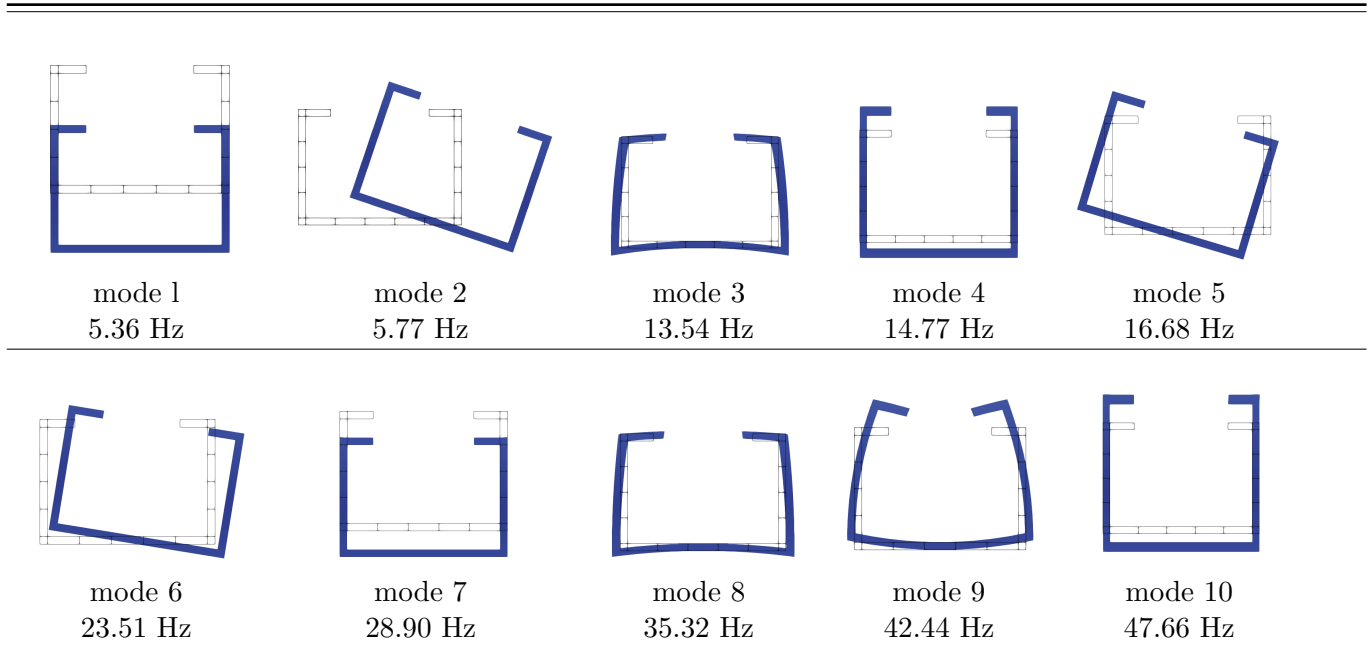


Table 19: Middle cross-sectional view of the first ten vibration mode shapes in the beam 4- arbitrary cross-section based on the model with 117 Lagrange points and 20B4 elements



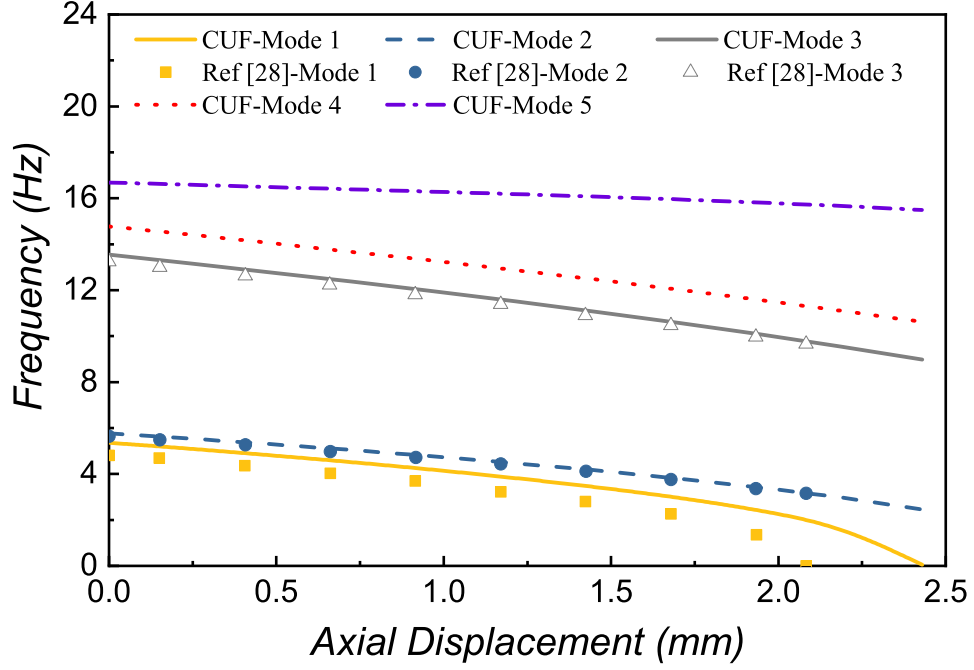


Figure 14: The comparison of the first five natural frequencies in the beam 4- arbitrary cross-section under progressive compressive loads based on the CUF model with 117 Lagrange points and Ref. [28]

Table 20: The variations of frequencies versus the applied axial displacements in the beam 4- arbitrary cross-section under progressive compressive loads based on the CUF-1D models and Ref. [28]

Axial Displacement (mm)	Frequency (Hz)- CUF			Frequency (Hz)-Ref. [28]		
	Mode 1	Mode 2	Mode 3	Mode 1	Mode 2	Mode 3
0.25	5.10	5.53	13.09	4.57	5.40	12.89
0.50	4.80	5.27	12.68	4.24	5.17	12.48
0.75	4.50	5.02	12.28	3.92	4.87	12.08
1.00	4.14	4.72	11.88	3.54	4.62	11.68
1.25	3.77	4.42	11.43	3.09	4.35	11.23
1.50	3.37	4.09	10.98	2.66	4.02	10.78
1.75	2.86	3.74	10.50	2.06	3.64	10.32

5 Conclusions

In this study, an efficient CUF-based method to investigate the vibrations and buckling of thin-walled beams with complex open cross-sections was presented. The effects of compressive loads on the natural frequencies of the beams subjected to the compression were evaluated. The CUF-based FE with the Taylor and Lagrange expansions were implemented and compared with the experimental results of the available literature and the numerical results by the shell models. For the cruciform beam, the values of natural frequencies from the available literature by using experimental methods and three numerical methods based on the thin shell, thick shell, and solid brick elements were compared, and the capability of the proposed cost-effective CUF-1D models to detect vibration modes and the cross-sectional deformations in this open cross-section thin-walled beam was shown.

The results of the thin cruciform beam also showed that for the beam with a thinner cross-section, the torsional modes with cross-sectional deformations might occur before the other bending modes, and many of the torsional modes might be missed by using the classical theories. Thus, the refined beam theories should be used in these cases for the accurate detection of vibration modes. Furthermore, refined theories based on Lagrange expansion are able to accurately describe the effects of compressive loads on the change of the natural frequencies.

The MAC analysis was conducted for the comparison of corresponding modes based on the classical and refined FE models based on the CUF-1D. It was noticed that the number of corresponding modes for the classical models such as Taylor order 1 was considerably less than other Lagrange models. In fact, many modes were lost by classical beam theories, and instead, they show rigid cross-section modes that did not really exist. Moreover, the results showed that although some modes might be corresponding to each other according to the MAC analysis, the values of natural frequencies based on the two models might show higher discrepancies. Therefore, the importance of the selection of structural theory capable of detecting the accurate eigenvalues and eigenvectors of the structural problem was highlighted. It should be noted that under the assumption that the first buckling and vibration modes are similar, the VCT can be used efficiently in order to extrapolate the buckling loads based on the decrease of the natural frequencies for the beam under progressive compressive loads.

References

- [1] A. H. Nayfeh and P. F. Pai. *Linear and nonlinear structural mechanics*. John Wiley & Sons, 2008.
- [2] L. Euler. Additamentum i: De curvas elasticis. *Leonhardi Euleri Opera omnia*, 1(24):231–297, 1911.
- [3] E. Bernoulli. De vibrationibus et sono laminarum elasticarum. *Commentarii Academiae Scientiarum Imperialis Petropolitanae*, 13(1741-3):105–20, 1751.
- [4] S. P. Timoshenko. Lxvi. on the correction for shear of the differential equation for transverse vibrations of prismatic bars. *The London, Edinburgh, and Dublin Philosophical Magazine and Journal of Science*, 41(245):744–746, 1921.
- [5] S. P. Timoshenko. X. on the transverse vibrations of bars of uniform cross-section. *The London, Edinburgh, and Dublin Philosophical Magazine and Journal of Science*, 43(253):125–131, 1922.
- [6] M. de Saint-Venant. *Mémoire sur la torsion des prismes: avec des considérations sur leur flexion ainsi que sur l'équilibre intérieur des solides élastiques en général: et des formules pratiques pour le calcul de leur résistance à divers efforts s'exerçant simultanément*. Imprimerie nationale, 1856.
- [7] M. de Saint-Venant. Venant. *Memoire sur la torsion des prismes, avec des considerations sur leur flexion*, *Mem, Savants Etrang*, 14:233–560, 1856.
- [8] W. Jrad. *Dynamic behavior of thin-walled beams: Analytical, numerical and experimental approaches*. PhD thesis, Université de Lorraine, 2019.
- [9] W. Jrad, F. Mohri, G. Robin, E. M. Daya, and J. Al-Hajjar. Analytical and finite element solutions of free and forced vibration of unrestrained and braced thin-walled beams. *Journal of Vibration and Control*, 26(5-6):255–276, 2020.

- [10] L. N. Virgin and R. H. Plaut. Effect of axial load on forced vibrations of beams. *Journal of Sound and Vibration*, 168(3):395–405, 1993.
- [11] L. N. Virgin. *Vibration of axially-loaded structures*. Cambridge University Press, 2007.
- [12] D. Kennedy and K. I. Lo. Critical buckling predictions for plates and stiffened panels from natural frequency measurements. In *Journal of Physics: Conference Series*, volume 1106, page 012018. IOP Publishing, 2018.
- [13] J. Singer, J. Arbocz, and T. Weller. *Buckling experiments*. Second Edition, 2002.
- [14] P. Cabral, E. Carrera, H. dos Santos, P. Galeb, A.o Pagani, D. Peeters, and A. P. Prado. Experimental and numerical vibration correlation of pre-stressed laminated reinforced panel. *Mechanics of Advanced Materials and Structures*, pages 1–13, 2020.
- [15] H. Abramovich. The vibration correlation technique—a reliable nondestructive method to predict buckling loads of thin walled structures. *Thin-Walled Structures*, page 107308, 2020.
- [16] G. Piana. *Vibrations and stability of axially and transversely loaded structures*. PhD thesis, Turin: Polytechnic University Turin, 2013.
- [17] S. Fässler. Axial load determination using modal analysis. 2014.
- [18] G. Piana, E. Lofrano, A. Manuello, G. Ruta, and A. Carpinteri. Compressive buckling for symmetric twb with non-zero warping stiffness. *Engineering Structures*, 135:246–258, 2017.
- [19] XY Li, XH Wang, YY Chen, Y Tan, and HJ Cao. Bending, buckling and free vibration of an axially loaded timoshenko beam with transition parameter: Direction of axial force. *International Journal of Mechanical Sciences*, 176:105545, 2020.
- [20] H. Abramovich. Natural frequencies of timoshenko beams under compressive axial loads. *Journal of Sound and Vibration*, 157(1):183–189, 1992.
- [21] A. Prokić and D. Lukić. Flexural-torsional vibration analysis of axially loaded thin-walled beam. *Journal of the Brazilian Society of Mechanical Sciences and Engineering*, 34(3):262–268, 2012.
- [22] A. Carpinteri, R. Malvano, A. Manuello, and G. Piana. Fundamental frequency evolution in slender beams subjected to imposed axial displacements. *Journal of Sound and Vibration*, 333(11):2390–2403, 2014.
- [23] Y. Q. Zhang, Y. Lu, S. L. Wang, and X. Liu. Vibration and buckling of a double-beam system under compressive axial loading. *Journal of Sound and Vibration*, 318(1-2):341–352, 2008.
- [24] X. Zhao, B. Chen, Y. H. Li, W. D. Zhu, F. J. Nkiegaing, and Y. B. Shao. Forced vibration analysis of timoshenko double-beam system under compressive axial load by means of green’s functions. *Journal of Sound and Vibration*, 464:115001, 2020.
- [25] G. Piana, E. Lofrano, A. Manuello, and G. Ruta. Natural frequencies and buckling of compressed non-symmetric thin-walled beams. *Thin-Walled Structures*, 111:189–196, 2017.
- [26] G. Piana, A. Carpinteri, E. Lofrano, and G. Ruta. Vibration and buckling of open TWBs with local weakening. *Procedia engineering*, 199:242–247, 2017.
- [27] G. Aquaro. *Torsional instability of open thin-walled beams: Numerical and experimental investigation*. PhD thesis, Politecnico di Torino, 2018.
- [28] Ł. Żmuda-Trzebiatowski. Investigation of natural frequencies of axially loaded thin-walled columns. In *MATEC Web of Conferences*, volume 219, page 02018. EDP Sciences, 2018.

- [29] B. Elkaibillah, A. Braikat, F. Mohri, and N. Damil. A one-dimensional model for computing forced nonlinear vibration of thin-walled composite beams with open variable cross-sections. *Thin-Walled Structures*, page 107211, 2020.
- [30] A. Pagani, R. Augello, and E. Carrera. Virtual vibration correlation technique (vct) for non-linear analysis of metallic and composite structures. In *ASME 2018 International Mechanical Engineering Congress and Exposition*. American Society of Mechanical Engineers Digital Collection, 2018.
- [31] A. Varello and E. Carrera. Free vibration response of thin and thick nonhomogeneous shells by refined one-dimensional analysis. *Journal of Vibration and Acoustics*, 136(6), 2014.
- [32] M. Cinefra, S. Valvano, and E. Carrera. A layer-wise mitc9 finite element for the free-vibration analysis of plates with piezo-patches. *International Journal of Smart and Nano Materials*, 6(2):85–104, 2015.
- [33] E. Zappino, T. Cavallo, and E. Carrera. Free vibration analysis of reinforced thin-walled plates and shells through various finite element models. *Mechanics of Advanced Materials and Structures*, 23(9):1005–1018, 2016.
- [34] E. Carrera, M. Petrolo, and P. Nali. Unified formulation applied to free vibrations finite element analysis of beams with arbitrary section. *Shock and Vibration*, 18(3):485–502, 2011.
- [35] M. Petrolo, E. Zappino, and E. Carrera. Refined free vibration analysis of one-dimensional structures with compact and bridge-like cross-sections. *Thin-Walled Structures*, 56:49–61, 2012.
- [36] E. Carrera, F. Miglioretti, and M. Petrolo. Computations and evaluations of higher-order theories for free vibration analysis of beams. *Journal of Sound and Vibration*, 331(19):4269–4284, 2012.
- [37] A. Pagani, F. Zangallo, and E. Carrera. Influence of non-structural localized inertia on free vibration response of thin-walled structures by variable kinematic beam formulations. *Shock and Vibration*, 2014, 2014.
- [38] M. Dan, A. Pagani, and E. Carrera. Free vibration analysis of simply supported beams with solid and thin-walled cross-sections using higher-order theories based on displacement variables. *Thin-Walled Structures*, 98:478–495, 2016.
- [39] X. Xu, N. Fallahi, and H. Yang. Efficient cuf-based fem analysis of thin-wall structures with lagrange polynomial expansion. *Mechanics of Advanced Materials and Structures*, pages 1–22, 2020.
- [40] A. Pagani, R. Augello, and E. Carrera. Frequency and mode change in the large deflection and post-buckling of compact and thin-walled beams. *Journal of Sound and Vibration*, 432:88–104, 2018.
- [41] E. Carrera, A. Pagani, and R. Augello. Effect of large displacements on the linearized vibration of composite beams. *International Journal of Non-Linear Mechanics*, 120:103390, 2020.
- [42] E. Carrera, M. Cinefra, M. Petrolo, and E. Zappino. *Finite element analysis of structures through unified formulation*. John Wiley & Sons, 2014.
- [43] Y. Kurylov and M. Amabili. Polynomial versus trigonometric expansions for nonlinear vibrations of circular cylindrical shells with different boundary conditions. *Journal of Sound and Vibration*, 329(9):1435–1449, 2010.

- [44] Y. Kurylov and M. Amabili. Nonlinear vibrations of clamped-free circular cylindrical shells. *Journal of sound and vibration*, 330(22):5363–5381, 2011.
- [45] E. Carrera, A. Pagani, and M. Petrolo. Classical, refined and component-wise theories for static analysis of reinforced-shell wing structures. *AIAA Journal*, 51(5):1255–1268, 2013.
- [46] E. Carrera and A. Pagani. Accurate response of wing structures to free vibration, load factors and non-structural masses. *AIAA Journal*, 54(1):227–241, 2016.
- [47] A. Pagani, E. Daneshkhah, X. Xu, and E. Carrera. Evaluation of geometrically nonlinear terms in the large-deflection and post-buckling analysis of isotropic rectangular plates. *International Journal of Non-Linear Mechanics*, 121:103461, 2020.
- [48] E. Carrera, A. Pagani, and M. Petrolo. Refined 1D finite elements for the analysis of secondary, primary, and complete civil engineering structures. *Journal of Structural Engineering*, 141:04014123/1–14, 2015.
- [49] E. Carrera and A. Pagani. Free vibration analysis of civil engineering structures by component-wise models. *Journal of Sound and Vibration*, 333(19):4597–4620, 2014.
- [50] K. J. Bathe. *Finite Element Procedure*. Prentice Hall, Upper Saddle River, New Jersey, USA, 1996.
- [51] E. Carrera and E. Zappino. Carrera unified formulation for free-vibration analysis of aircraft structures. *AIAA Journal*, 54(1):280–292, 2016.
- [52] R. J. Allemang and D. L. Brown. A correlation coefficient for modal vector analysis. In *Proceedings of the 1st international modal analysis conference*, volume 1, pages 110–116. SEM Orlando, 1982.
- [53] R. J. Allemang. The modal assurance criterion—twenty years of use and abuse. *Sound and vibration*, 37(8):14–23, 2003.
- [54] M. Pastor, M. Binda, and T. Harčarik. Modal assurance criterion. *Procedia Engineering*, 48:543–548, 2012.